Time-resolved CMOS SPAD arrays: architectures, applications and perspectives

Federica Villa, Rudi Lussana, Davide Portaluppi, Alberto Tosi, Franco Zappa
Politecnico di Milano, Dipartimento di Elettronica, Informazione e Bioingegneria,
Piazza Leonardo da Vinci 32, Milano I-20133 (Italy)
federica.villa@polimi.it

ABSTRACT

SPADs (Single-Photon Avalanche Diodes) are the viable photodetectors for most single-photon counting and photon-timing applications. Some custom SPAD and many complementary metal-oxide semiconductor (CMOS) SPADs have been reported in literature, with quite different performance and some excelling in just few of them, but often at different operating conditions. Proper performance assessment can be done through figures of merit able to summarize the typical SPAD performance (i.e. photon detection efficiency, dark counting rate, afterpulsing probability, hold-off time, and timing jitter) and to identify a proper metric for SPAD comparisons, when used either as single pixel detectors or in imaging arrays. We present a comparison among some imager architectures and SPAD detectors and arrays in either photon-counting, timing, or imaging applications.

Keywords: Single-photon avalanche diode (SPAD), photon counting, CMOS imagers, figure of merit.

1. INTRODUCTION

Since ‘60s, Single-Photon Avalanche Diodes (SPADs) have been deeply studied and used in several fields where single-photon sensitivity is required such as fluorescence correlation spectroscopy (FCS) [1], fluorescence lifetime imaging (FLIM) [2], positron emission tomography (PET) [3], as well as laser (LIDAR/LADAR) [4] and 3-D optical ranging [5]. In all these applications, the intensity and time-dependent waveform of very faint optical signals can be acquired by counting photons (photon-counting) in real-time, within time-bins down to the microsecond time scale. Also, the waveforms of very fast events, down to the picosecond time-scale, can be reconstructed by repetitively acquiring the arrival time (photon-timing), exploiting Time-Correlated Single-Photon Counting (TCSPC) for building the histogram.

Although many single-photon sensitive devices already existed, SPADs have gained attention because of some advantages over photomultiplier tubes (PMTs) and multi-channel plates (MCPs), which require high bias voltages, are bulky and sensitive to magnetic fields, and cannot be integrated with complementary metal-oxide semiconductor (CMOS) electronics. Conversely, SPADs are small, rugged, easy to integrate in large array, and are insensitive to magnetic fields, making them suitable for medicine and space application [6]. Until ten years ago, SPADs were fabricated solely through fully custom processes, whose flexibility provided devices with thick depleted regions, engineered electric fields, and dedicated annealing steps and gettering processes for minimizing lattice damages for improving noise, yield, and uniformity. Custom SPADs provide best-in-class performance in terms of detection efficiency, noise and timing jitter [7]-[12]. However, because of dedicated processes and the impossibility to integrate proper quenching and processing electronics with the detector, custom SPADs are best suited for single- or some- (up to about a hundred) pixel arrays [13].

From the early 2000s onwards, it was possible to exploit standard CMOS technologies to fabricate SPADs, with the main advantage of monolithic integration on the same chip of photodetectors, analog avalanche sensing and quenching electronics, and digital electronics for implementing smart photon-counting and photon-timing on-chip processing, which are a viable solution to bulky and expensive intensified (I-CCDs) or electron-multiplying charge-coupled devices (EM-CCDs).

In the last years, many groups worldwide developed different SPAD structures in different CMOS technology nodes [14] -[28] for coping with the different issues, but with measurements acquired in different experimental conditions (e.g. breakdown voltage, excess bias, hold-off time, average count rate, wavelength, etc.), which better maximized the target data, and often claimed to have reached the novel state-of-the-art performance in one or another parameter. In such a maze of variables and measurements, it is difficult to make a fair comparison between different SPAD designs and CMOS technologies, and to envision a clear trend, unless a subset of representative parameters is found. To this purpose, we proposed [29] a comprehensive Figure-of-Merit (FoM) based on well-assessed typical SPAD performance, like photon detection efficiency, noise, dead-time, timing jitter, fill-factor [30], and other well-known quality meters, like Signal-to-Noise Ratio, Noise Equivalent Power, and Detectivity, in different application fields (photon-counting and photon-timing) and either as single pixels or as SPAD array imagers.

2. CMOS SPAD PERFORMANCE

Photon Detection Efficiency (PDE) is defined as the ratio of the number of detected photons and the number of photons incident on the photoactive area and it depends on absorption probability and on triggering efficiency [30]. Apart from signal fluctuations due to its own Poisson statistics, SPAD's main noise source is due to dark counts, which are either uncorrelated or correlated to signal photons. The uncorrelated contribution is due to ignitions caused by carriers generated through either Shockley-Read-Hall processes, trap-assisted tunneling (TAT), or Poole-Frenkel emission and is referred to as Dark Counting Rate (DCR) [30]. Instead, correlated noise comes from different sources, such as optical and electrical crosstalk (among different pixels) and afterpulsing (within the same pixel). The latter is caused by carriers that get trapped during an avalanche current pulse and are then released, when the SPAD is biased above breakdown (V_{BD}), thus igniting an "afterpulse". In order to reduce the afterpulsing probability (P_{AP}), a dead-time T_{DEAD}, (from tens to hundreds of nanoseconds) is enforced to the SPAD after each ignition, for waiting for the trapped carriers release. Finally, the SPAD timing jitter (photon-timing precision) is the statistical spread of output pulse on-set compared to the true photon arrival time [31] and is quoted by the Full-Width at Half Maximum (FWHM) of the distribution histogram (see Fig. 1).

Single-photon detectors are exploited in three main approaches, namely photon-counting (for measuring the intensity of slowly varying optical signals, in the µs range), photon-timing (for reconstructing very fast optical waveforms, in the ps range, or the "time-of-flight") and photon-imaging (for acquiring one- or two-dimensional images of a specimen). For the former two, one or few dozen independent detectors usually suffice, whereas imaging requires large arrays at least hundreds of detectors, hence pixel pitch and fill-factor do play an important role.

In photon-counting, SPAD performance can be quoted with the following FoM [29]:

$$FoM_C = PDE \cdot \frac{\sqrt{Area}}{\sqrt{DCR}} \cdot \frac{1 - P_{AP}}{T_{DEAD}}$$

where the subscript "$_C$" stands for "counting" application, Area is the SPAD active area, and $1/T_{DEAD}$ is the maximum achievable photon flux. Table I in Ref. [29] shows the FOM_C values computed for a large number of custom SPADs, CMOS SPADs, and SiPMs; as can be seen, typical values range from 0.01 $\sqrt{count} \cdot m$ to 1,000 $\sqrt{count} \cdot m$. Of course, since PDE depends on photon wavelength, spot FoM_C values could be quoted for application-specific wavelengths or an average PDE value could be used as representative over the range of interest.

In photon-timing, SPAD performance can be quoted with the following FoM [29]:

$$FoM_T = PDE \cdot \frac{Area}{DCR} \cdot \frac{1 - P_{AP}}{T_{DEAD}} \cdot \frac{1}{FWHM}$$

where the subscript "$_T$" stands for "timing" application, As for FOM_C, Table I in Ref. [29] shows also the FOM_T values computed for a large number of custom SPADs, CMOS SPADs, and SiPMs; as can be seen, typical values range from 1 m^2/s to 10^8 m^2/s. Also similar to FoM_C, PDE should be evaluated at the specific wavelength of the desired application or the PDE average could be computed over the range of interest. Concerning SiPMs, Ref. [29] provides some comments and more insight.

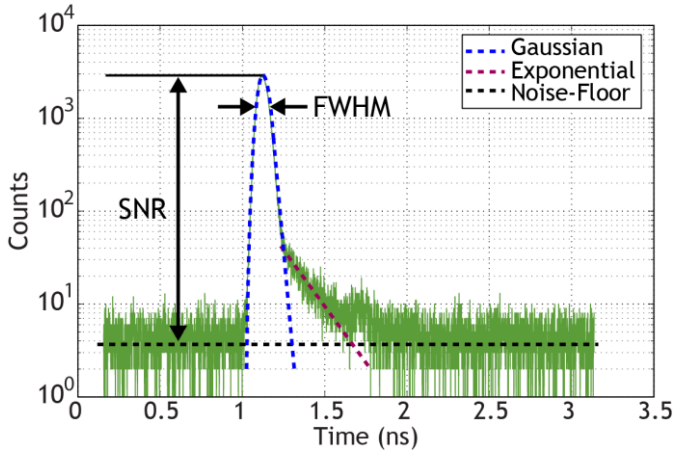

Fig. 1. Typical timing waveform of a SPAD, with its Gaussian intrinsic "fast" response, with its Full-Width at Half Maximum, and the "slow" diffusion tail response (in dashed red line), whose attack (distance from the peak) and duration (the time constant) could adversely impact the SPAD timing performance, given the desired Signal-to-Noise ratio SNR, defined as the ratio between the timing peak and the noise background.

Concerning imaging applications, CMOS SPADs typically have worst performance than custom SPADs, but they can be integrated together with on-chip electronics, resulting in monolithic large arrays with thousands of pixels, which can provide either 2D, 3D (distance-resolved), or time-resolved images and movies. In most imaging applications, the sensor is used to count the number of incoming photons, either in free-running or in gated-mode. For this reason, the imaging FoM_I can be derived starting from FoM_C, by further adding three fundamental parameters for array imagers: i) fill-factor; ii) number of pixels; iii) maximum frame-rate. Another important item is crosstalk probability among pixels, but this value is not usually reported in literature as it is generally negligible, thus we will not consider it. Hence, FoM_I should take into account efficiency, noise, fill-factor (FF), number of pixels (N), maximum frame-rate (f_{MAX}), and maximum count rate:

$$FoM_I = PDE \cdot \frac{\Phi_{MAX}}{\sqrt{DCR}} \cdot FF \cdot N \cdot f_{MAX}$$

Table III in Ref. [29] shows the FOM_I values computed for a large number of CMOS SPAD imagers; as can be seen, typical values range from $5\ \sqrt{count} \cdot kframe/s$ to $10^5\ \sqrt{count} \cdot kframe/s$.

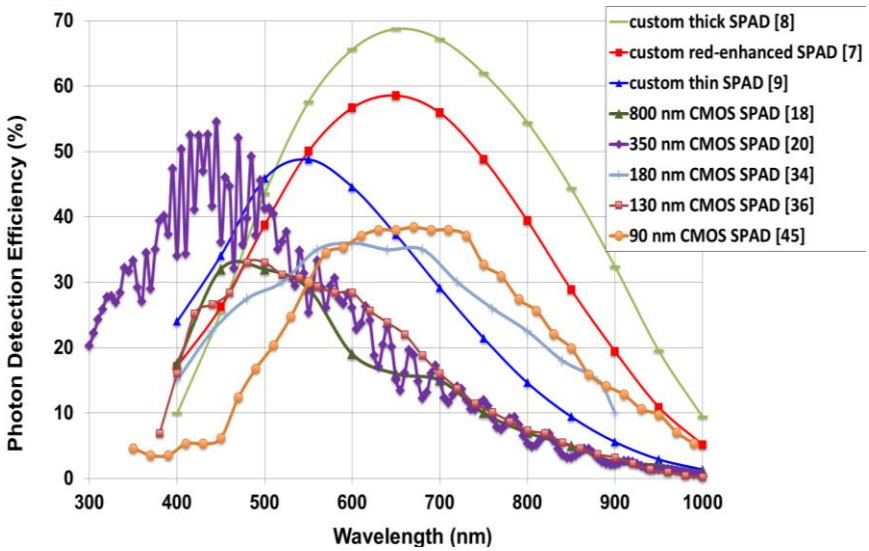

Fig. 2: Spectral Photon Detection Efficiency for some CMOS technologies and custom SPADs for comparison (see Ref. [29] for details).

We reviewed a large number of papers on Silicon SPADs and SiPMs presented in scientific literature or commercially available [29], representing the state-of-the-art SPAD-based pixels, fabricated in both custom and CMOS technologies, with their main parameters and corresponding FoM_C and FoM_T values. The analyzed SPAD technologies are seven: custom technologies, two submicron (0.8 µm and 0.35 µm), and three deep-submicron (0.18 µm, 0.13 µm and 90 nm) technologies, and single-cells of digital and analog SiPMs. Among CMOS SPADs, the performance of "older" nodes show minor spread: this is related to the fabrication of almost "standard" structure devices (i.e. shallow p-diffusion in n-well, with p-doped guard-ring). On the contrary, for scaled devices, different structures were proposed: some implemented a standard structure device; others (e.g. [20] and [26]) presented a reverse n+/p-well structure; while these structures are not amenable to scaling and thus to improve fill-factor in SPAD arrays, [19] presented an STI-bounded SPAD, where Shallow Trenches Isolation (STI) are used as guard-ring in place of low-doped diffusions, thus allowing to shrink SPAD dimension down to 2 µm. Nonetheless, all those structures proved to be very noisy because of the high doping concentrations and consequently high electric fields (typical of scaled technologies), which boost tunneling and field-enhanced carrier generation effects.

Fig. 2 shows the spectral PDE of custom and CMOS highest efficiency SPADs. Thick custom SPADs present higher PDE in the Near Infra-Red (NIR) because of the wider absorption region (and higher V_{BD}) than CMOS ones. The SPAD in Ref. [14] (0.35µm technology) reaches the highest peak PDE in the Near Ultra-Violet (NUV) thanks to the use of shallow diffusions that defines the SPAD active volume, but the efficiency drops down in the NIR. Almost no PDE trend is visible moving from submicron to deep sub-micron technologies: indeed the PDE is strictly related to the SPAD design and only marginally dependent on the employed technology node. For instance, the aforementioned alternative deep sub-micron implementations reach lower fields and have wider depleted zone, thus exhibiting enhanced and broader spectral response. Conversely, lower PDE values are achieved by standard p+/n-well junction, whose high doping concentrations cause a shrink of the depleted layer width.

Concerning the imaging performance,

Table I reports the performance of SPAD arrays designed only for photon counting imaging applications [5], [15], [17], [32]-[38]. The table does not include arrays for timing applications with integrated TDC (Time-to-Digital Converters), because the performance of these sensors depends much more on the time electronics than on the SPADs itself. These time-resolved imagers will be discussed in the following Section.

3. TIME-RESOLVED IMAGERS

At POLIMI we developed microelectronic sensor chip comprising arrays of smart-pixels, with SPADs and digital counters for configurable photon counting applications [39] and also more complex time-resolved imagers with SPADs and photon-timing electronics for acquiring the arrival time of single photons [40]. The smart pixel for time-resolved imagers is usually based on a SPAD detector and a TDC. We developed arrays with different sizes (32x32, 16x32, 60x1), SPAD diameters (30 µm – 135 µm) and fill-factors, in a 0.35 µm high-voltage CMOS technology, automotive qualified.

Table I: Main imager parameters for several SPAD arrays and their imaging figure of merit.

Ref.	Shutter	Processing	# Pixels	Bits / pixel	Pitch (µm)	FF (%)	PDE (%)	DCR (cps)	f_{MAX} (kfps)	Power (mW)	FoM_I (√count·kframe/s)
[32]	-	Multiplex.	32×32	1	58	1.14	12	350	70	6	131
[33]	-	Event-driven	64×48	1	45	9.6	26	370	70	-	4,465
[15]	-	Event-driven	4×112	1	25	12.57	40	750	70	-	225
[5]	Global	Parallel	64×32	9+9+9	150	3.14	50	100	100	50	15,434
[34]	Rolling	Parallel	60×48	8+8	85	0.53	35	245	46	35	393
[17]	Global	Multiplex.	64×4	8	26	34	32	1000	150	200	661
[35]	Rolling	Multiplex.	32×32	1	75	8	42.4	7000	70	-	116
[36] I	-	Multiplex.	1024×8	1	24	4.90	6	80	0.95	-	41
[36] II	-	Multiplex.	1024×8	1	24	44.30	23	5700	0.95	-	168
[37]	-	Multiplex.	128×96	10	44.65	3.19	28	100	70	40	7,685
[38]	Rolling	Multiplex.	512×128	1	24	5	46	366	156	1,650	122,911

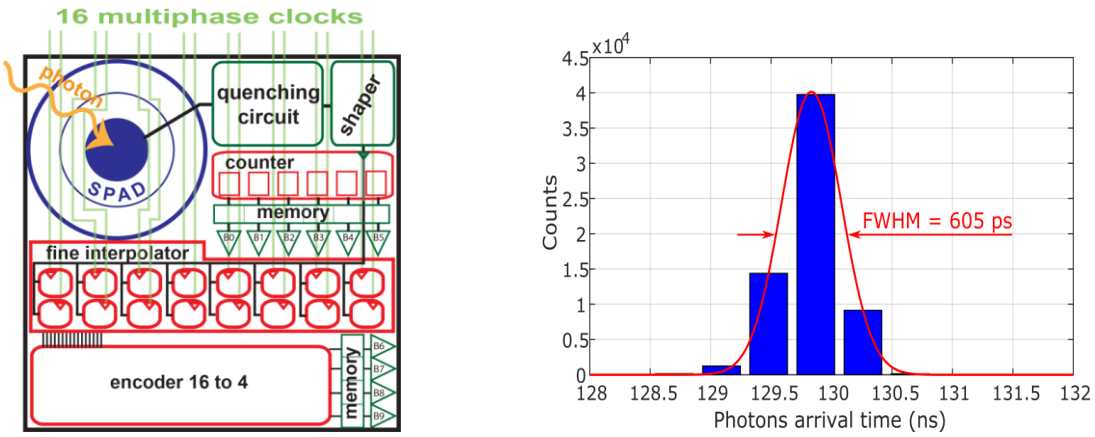

Fig. 3: Example of one pixel of a 32x32 time-resolved imager, containing a 30 µm SPAD, with a 150 µm pitch, 3.14% fill-factor, a 10-bit TDC for "photon timing" (e.g. FLIM and TOF LIDAR) with 390 ps LSB, 400 ns FSR, a 6-bit counter for "photon-counting" (2D imaging) at 100,000 frame/s.

Usually squared arrays are interesting for 3D ranging applications where scanning must be avoided; while linear arrays are more suitable for bioimaging, microscopy, and spectroscopy applications, since they can reach higher frame-rate and provide higher fill-factor, though they provide just one or a few rows of detectors. For example linear arrays can be investigated in portable time-resolved Raman Spectroscopy systems, becoming the enabling technology to distinguish Raman stimulated emission from fluorescence background, by exploiting the arrival time of emitted photons.

In the time-resolved SPAD imager discussed in Ref. [40], both photon-counting and photon-timing electronics have been implemented within the sensor. In photon-counting mode, for 2D imaging, a 6-bit counter provide a result proportional to the intensity of the light emitted/reflected by the objects in the scene or the biological specimen under observation. In photon-timing mode, for 3D distance-resolved ranging, the integrated TDC is split in coarse counter (for providing a long dynamic range) and a fine interpolator (for sub-nanosecond time stamping), in order to measure the accurate time-of-flight or fluorescence decay of the sample. The time bin is adjustable from 312 ps (with 10 bit resolution) to 10 ns (with 6 bit resolution), i.e. from 5 cm to 3 m distance resolution in 3D ranging, when using a 100 MHz reference clock. The power consumption of the chip at the maximum resolution and speed is lower than 1 W, whereas the total power consumption of the entire camera is 2.5 W. Compared to other arrays of SPADs and TDCs presented in literature, this sensor shows better linearity and state-of-the-art SPAD performance [29] [39] [40], though timing resolution was kept lower to allow the integration of one TDC per SPAD, with no need of any multiplexing and photon loss. The depth precision in 3D ranging applications is improved by accumulating a large number of conversion (> 500) and then computing the centroid of the acquired histogram of photons arrival times, thus reaching millimeter precisions, as shown in Fig. 4.

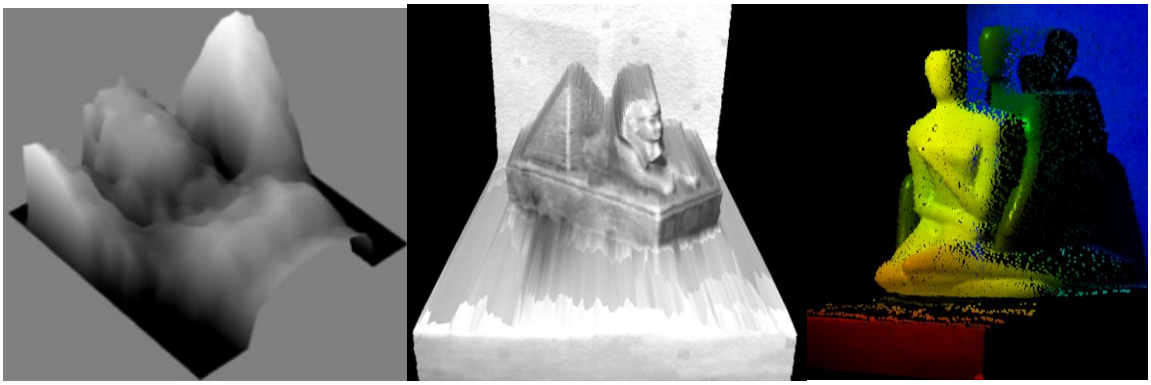

Fig. 4: Example of 3D acquisitions with the time-resolved SPAD imager reported in Ref. [40] when using a 90 mW laser power at 670 nm wavelength, at 10 m distance from the objects (namely a person, a small sphynx and another statue, both about 20cm in height), reaching 0.4 mmRMS precision, after 250 ms integration time [41]. The image at the center and at the right hand side have been acquired by scanning the 32x32 imager 10 x 5 times, in order to achieve a final resolution of 320x160.

Table II: Comparison of some time-resolved SPAD imagers reported in literature. The first one it the imager reported in Ref. [40].

Work	Technology [nm]	Architecture	DCR per area @20°C [Hz/μ²]	Peak PDE [%]	Fill Factor [%]	TDC LSB [ps]	TDC range [ns]	DNL pp [%LSB]	INL pp [%LSB]	Precision rms [ps]
SPADlab Array	**350**	**32x32 SPAD 32x32 TDC**	**0.021**	**50**	**3.14**	**390**	**400**	±5% **(19.5 ps)**	±22% **(86 ps)**	**257**
M. Gersbach, 2012	130	32x32 SPAD 32x32 TDC	189	35	2.3	119	120	±40% (48 ps)	±120% (150 ps)	101.3
C. Veerappan, 2011	130	160x128 SPAD 160x128 TDC	318	12	1	55	55	±30% (17 ps)	±200% (110 ps)	59.4
C. Niclass, 2013	180	340x96 SPAD 32 TDC	6	20	14	97.6	100	±8% (8 ps)	±189% (185 ps)	106.2
D. Stoppa, 2009	130	32x32 SPAD 32x32 TAC 32x32 ADC	1273	35	3.14	160	20.5	±35% (56 ps)	±95% (152 ps)	255
M. Perenzoni, 2017	150	64x64 dSiPM (4x2 SPADs each) 64x64 TDC	59	?	26.5	250	13884	±20% (50 ps)	±400% (1 ns)	331

In literature, other time-resolved SPAD imagers have been reported so far. Table II summarizes the performance of some of them. As can be seen, the number of pixel is always limited to some kpixels for technology nodes between 0.35 μm and 150 nm. Other implementations in deep submicron nodes are being published in the last years, with more complex electronics and higher pixel count, but usually poorer SPAD detection performance. For example the best performing timing electronics in Table II is reached with a poor 12% peak PDE and 1% fill-factor, while the highest fill-factor of 26.5% results in the worse TDC precision.

The timing electronics could be based on Time-to-Analog Converters (TACs), which are best-in-class in timing performance and linearity (e.g., in Ref. [17], with 160 ps LSB). However, Time-to-Digital Converters (TDCs) are much smaller and provide easier integrability. Moreover TDCs offer excellent linearity if sliding-scale is exploited. Concerning the array readout mode, it can be conceived in two different approaches. In the "time-driven" technique, every pixel is readout at every frame, so to result in smaller complexity, but longer readout time. Instead, "event-driven" arrays rely on the readout of only those pixels that experienced a photon detection (or an unwelcome dark-count event), while all other pixels are skipped, thus resulting in higher frame rate [e.g. in Ref. [15] and Ref. [33]). Finally, the placement of the timing electronics strongly impacts on the overall fill-factor and architecture scalability. When integrated into each pixel, the architecture offers high parallelism, high throughput and easier microelectronics layout. Instead, when the timing electronics is shared between neighboring pixels, it requires lower area occupation, but it is suitable only as long as the detection rate is sufficiently low, not to cause too high photon loss.

In some applications requiring photon timing information, the unwelcome contribution of a high background (e.g. the sun light or the light "polluted" environment) could drastically corrupt the overall functionality of the time-resolved SPAD imager, so sensitive to light to cause saturation of the detector or of the timing electronics. For example, in 3D ranging sensor for autonomous driving, the imager must be operative even in extremely challenging environmental conditions, under direct sun light, in front of the high beams of incoming vehicles, and so on. Possible solutions should be implemented on the "optical" path, e.g. through narrow-wavelength filters centred at the laser illumination wavelength, and even on the chip design. For example, by putting more SPADs in parallel could allow to implement smart detection technique, where the TDC be triggered only when two or more SPADs are triggered at the same time, within a sub-nanosecond coincidence window. In this way, the 3D-ranging chip could possibly reject background photons, being usually uncorrelated and random in arrival time, while back-reflected signal photons concurrently trigger the parallelized SPADs. Some papers are being presented in literature based on this technique.

Conclusions

We discussed the performance of CMOS SPAD detectors, by analysing the main SPAD parameters and the figures-of-merit proposed in Ref. [29] to assess the performance in real photon-timing, photon-counting and imaging applications, with a single (or a few) pixel or a full CMOS SPAD array imager for the acquisition of both 2D photon-counting and 3D photon-timing images. CMOS SPADs are the only choice to provide real imaging at the single-photon level. Among different CMOS SPADs, state-of-the-art devices are designed in 0.35 μm technologies, where very low DCR and very large (30-100μm) SPAD diameters are fabricated, at the expenses of large (5 mm x 5 mm) chips with just 1k – 2k pixel count. Instead, more scaled technologies allow exploiting advanced cross-sections, hence benefiting of much smaller pitch, chip dimensions, and higher (up to 10k-15k) pixel-count, but at the drawback of very small SPAD dimensions (few micrometer diameters) and higher noise per active area.

REFERENCES

[1] R. A. Colyer, G. Scalia, I. Rech, A. Gulinatti, M. Ghioni, et al., "High-throughput FCS using an LCOS spatial light modulator and an 8×1 SPAD array," Biomedical Opt. Express, vol. 1, no. 5, pp.1408-1431, Dec. 2010.

[2] M. Vitali, D. Bronzi, A. J. Krmpot, S. N. Nikolic, F.-J. Schmitt, C. Junghans, S. Tisa, T. Friedrich, V. Vukojevic, L. Terenius, F. Zappa, and R. Rigler, "A Single-Photon Avalanche Camera for Fluorescence Lifetime Imaging Microscopy and Correlation Spectroscopy," IEEE J. Sel. Topics Quantum Electron., vol. 20, no. 6, pp. 344-353, Nov.-Dec. 2014.

[3] M. E. Daube-Witherspoon, S. Matej, M.E. Werner, S. Surti, J.S. Karp, "Comparison of list-mode and DIRECT approaches for time-of-flight PET reconstruction," IEEE Nucl. Science Symp. Conf. Record. pp. 2252-2258, 2010.

[4] M. A. Albota, R. M. Heinrichs, D. G. Kocher, D. G. Fouche, B. E. Player, M. E. O'Brien, B. F. Aull, J. J. Zayhowski, J. Mooney, B. C. Willard, and R. R. Carlson, "Three-dimensional imaging laser radar with a photon-counting avalanche photodiode array and microchip laser," Appl. Opt., vol. 41, pp. 7671–7678, 2002.

[5] D. Bronzi, F. Villa, S. Tisa, A. Tosi, F. Zappa, D. Durini, S. Weyers, and W. Brockherde, "100 000 Frames/s 64 × 32 Single-Photon Detector Array for 2-D Imaging and 3-D Ranging," IEEE J. Sel. Topics Quantum Electron., vol. 20, no. 6, pp. 354-363, Nov.-Dec. 2014.

[6] I. Prochazka, K. Hamal, B. Sopko, "Recent achievements in single photon detectors and their applications," J. Mod. Optic., vol. 51, no. 9-10, pp. 1289-1313, Jul. 2004.

[7] A. Gulinatti, I. Rech, F. Panzeri, C. Cammi, P. Maccagnani, M. Ghioni and S. Cova, "New silicon SPAD technology for enhanced red-sensitivity, high-resolution timing and system integration," J. Mod. Optic., vol. 59, no. 17, 1489-1499, 2012.

[8] www.excelitas.com/Downloads/DTS_SPCM-AQRH.pdf

[9] www.micro-photon-devices.com/Docs/Datasheet/PDM.pdf

[10] www.micro-photon-devices.com/Docs/Datasheet/PDM-R.pdf

[11] www.idquantique.com/instrumentation/product/id120-silicon-apd-single-photon-detector.html

[12] www.lasercomponents.com/de-en/photodiodes/avalanche-photodiodes/single-photon-counting-modules/

[13] S. Tisa, F. Zappa, A. Tosi, S. Cova, "Electronics for single photon avalanche diode arrays", Sensors and Actuators A, vol. 140, no. 1, pp. 113-122, Oct. 2007.

[14] F. Villa, D. Bronzi, Y. Zou, C. Scarcella, G. Boso, S. Tisa, A. Tosi, F. Zappa, D. Durini, S. Weyers, W. Brockherde, U. Paschen, "CMOS SPADs with up to 500 μm diameter and 55% detection efficiency at 420 nm," J. Mod. Opt., vol. 61, n. 2, pp. 102-115, Jan. 2014.

[15] C. Niclass, M. Sergio, and E. Charbon, "A single-photon avalanche diode array fabricated in 0.35 μm CMOS and based on an event-driven readout for TCSPC experiments," in Proc. SPIE 6372, 63720S, Oct. 2006.

[16] D. Mosconi, D. Stoppa, L. Pancheri, L. Gonzo, and A. Simoni, "CMOS single-photon avalanche diode array for time-resolved fluorescence detection," Proc. ESSCIRC 2006, pp. 564-567, Sep. 2006.

[17] L. Pancheri, and D. Stoppa, "A SPAD-based pixel linear array for high-speed time-gated fluorescence lifetime imaging," Proc. ESSCIRC 2009, pp. 428-431, Sep. 2009.

[18] E. Vilella, O. Alonso, A. Montiel, A. Vilà, A. Diéguez, "A Low-Noise Time-Gated Single-Photon Detector in a HV-CMOS Technology for Triggered Imaging," Sensors and Actuators A Physical, vol. 201, pp. 342-351, Oct. 2013.,

[19] H. Finkelstein, M.J. Hsu, and S.C. Esener, "STI-Bounded Single-Photon Avalanche Diode in a Deep-Submicrometer CMOS Technology," IEEE Electron Device Lett., vol. 27, no. 11, pp. 888-889, Nov. 2006.

[20] S. Mandai, M. Fishburn, Y. Maruyama, and E. Charbon, "A wide spectral range single-photon avalanche diode fabricated in an advanced 180 nm CMOS technology," Opt. Express, vol.20, no. 6, pp. 5849-5857 Mar. 2012.
[21] C. Niclass, M. Gersbach, R. Henderson, L. Grant, and E. Charbon, "A single photon avalanche diode implemented in 130-nm cmos technology," IEEE J. Select. Topics Quantum Electron., vol. 13, no. 4, pp. 863-869, Aug. 2007.
[22] M. Gersbach, J. Richardson, E. Mazaleyart, S. Hardillier, C. Niclass, R. Henderson, L. Grant, and E. Charbon, "A low-noise single-photon detector implemented in a 130nm CMOS imaging process," Proc. Solid-State Sensors, Actuators and Microsystems Conference, vol. 53, no. 7, pp. 803-808, Jul. 2009.
[23] R. M. Field, J. Lary, J. Cohn, L. Paninski, K. L. Shepard, "A low-noise, single-photon avalanche diode in standard 0.13μm complementary metal-oxide-semiconductor process," Appl. Phys. Lett., vol. 97, no. 211111, pp. 1-3, 2010.
[24] C. Veerappan, J. Richardson, R. Walker, Li Day-Uey, M. W. Fishburn, Y. Maruyama, D. Stoppa, F. Borghetti, M. Gersbach, R. K. Henderson, and E. Charbon, "A 160×128 single-photon image sensor with on-pixel 55ps 10b time-to-digital converter," Proc. ISSCC 2011, pp.312-314, 2011.
[25] M. Gersbach, Y. Maruyama, R. Trimananda, M. W. Fishburn, D. Stoppa, J. A. Richardson, R. Walker, R. Henderson, and E. Charbon, "A Time-Resolved, Low-Noise Single-Photon Image Sensor Fabricated in Deep-Submicron CMOS Technology," IEEE J. Solid-State Circuits, vol. 47, no. 6, pp. 1394-1407, Jun. 2012.
[26] M.A. Karami, M. Gersbach, H.J. Yoon, and E. Charbon, "A new single-photon avalanche diode in 90nm standard CMOS technology," Opt. Express, vol. 18, no. 21, pp. 22158-22166, Oct. 2010.
[27] B. Nouri, M. Dandin, and P. Abshire, "Large-area low-noise Single-Photon Avalanche Diodes in standard CMOS," Proc. IEEE Sensors, pp.1-5, Oct. 2012.
[28] T. Leitner, A. Feiningstein, R. Turchetta, R. Coath, S. Chick, G. Visokolov, V. Savuskan, M. Javitt, L. Gal, I. Brouk, S. Bar-Lev, and Y. Nemirovsky, "Measurements and Simulations of Low Dark Count Rate Single Photon Avalanche Diode Device in a Low Voltage 180-nm CMOS Image Sensor Technology," IEEE Trans. Electron Devices, vol. 60, no. 6, pp. 1982,1988, Jun. 2013.
[29] D. Bronzi, F. Villa, S. Tisa, A. Tosi, F. Zappa, "SPAD Figures of merit for photon-counting, photon-timing, and imaging applications: A review," IEEE Sensors Journal 16 (1), 3-12, 2016.
[30] F. Zappa, S. Tisa, A. Tosi, and S. Cova, "Principles and features of single-photon avalanche diode arrays," Sensors and Actuators A, vol. 170, no. 7, pp. 103-112, Oct. 2007.
[31] S. Cova, A. Lacaita, M. Ghioni, G. Ripamonti, and T. A. Louis, "20 ps timing resolution with Single Photon Avalanche Diodes," Rev. Sci. Instrum., vol. 60, no. 6 pp. 1104-1110, Jun. 1989.
[32] C. Niclass, A. Rochas, P. Besse, and E. Charbon, "Design and Characterization of a CMOS 3-D Image Sensor Based on Single Photon Avalanche Diodes", IEEE J. Solid-State Circuits, vol. 40, no. 9, Sep. 2005.
[33] C. Niclass, M. Sergio, and E. Charbon, "A CMOS 64×48 Single Photon Avalanche Diode Array with Event-Driven Readout", Proc. IEEE ESSCIRC, pp. 556-559, 2006.
[34] C. Niclass, C. Favi, T. Kluter, F. Monnier, and E. Charbon, "Single-Photon Synchronous Detection", S IEEE J. Solid-State Circuits, vol. 44, no. 7, pp. 1977-1989, Jul. 2009.
[35] A. L. Bernassau, M. Al-Rawhani, J. Beeley, and D. R. S. Cumming, "Integrated ultrasonic particle positioning and low excitation light fluorescence imaging," Appl. Phys. Lett., Vol. 103, 2013.
[36] Y. Maruyama, J. Blacksberg, and E. Charbon, "A 1024×8, 700-ps Time Gated SPAD Line Sensor for Planetary Surface Exploration With Laser Raman Spectroscopy and LIBS", IEEE J. Solid-State Circuits, vol. 49, no. 1, pp. 179-189, 2014.
[37] R. J. Walker, J. A. Richardson, and R. K. Henderson, "A 128×96 pixel event-driven phase-domain ΔΣ-based fully digital 3D camera in 0.13μm CMOS imaging technology," Proc. IEEE ISSCC Dig. Tech. Papers, pp. 410-412, Feb. 2011.
[38] S. Burri, Y. Maruyama, X. Michalet, F. Regazzoni, C. Bruschini, and E. Charbon, "Architecture and applications of a high resolution gated SPAD image sensor," Opt. Express, vol. 22, no. 14, pp. 17573-17589, Jul. 2014.
[39] D. Bronzi, F. Villa, S. Tisa, A. Tosi, F. Zappa, D. Durini, S. Weyers, et al, "100 000 frames/s 64× 32 single-photon detector array for 2-D imaging and 3-D ranging," IEEE journal of selected topics in quantum electronics 20 (6), 354-363, 2014.
[40] F. Villa, R. Lussana, D. Bronzi, S. Tisa, A. Tosi, F. Zappa, A. Dalla Mora, et al, "CMOS imager with 1024 SPADs and TDCs for single-photon timing and 3-D time-of-flight," IEEE journal of selected topics in quantum electronics 20 (6), 364-373, 2014.
[41] R Lussana, F Villa, A Dalla Mora, D Contini, A Tosi, F Zappa, "Enhanced single-photon time-of-flight 3D ranging," Optics Express 23 (19), 24962-24973, 2015.